

Synthesis of Some Tetrahedral Mixed Metal Platinum-Gold Clusters and the X-ray Crystal Structure of $[\{Au(PCy_3)\}\{Pt_3(\mu-CNXyl)_2(\mu-CO)(CNXyl)(PCy_3)_2\}][PF_6]$

Daniel Imhof, Urs Burckhardt, Klaus-Hermann Dahmen,* and Heinz Rügger

Laboratorium für anorganische Chemie,
ETH Zürich, Universitätsstrasse 6, CH-8092 Zürich, Switzerland

Tobias Gerfin and Volker Gramlich

Institut für Kristallographie und Petrographie,
ETH Zürich, Sonneggstrasse 5, CH-8092 Zürich, Switzerland

Received April 12, 1993*

The cluster compounds $[Pt_3(\mu-CNXyl)_2(\mu-CO)(CNXyl)(PCy_3)_2]$ (1) and $[Pt_3(\mu-CNXyl)_3(CNXyl)_2(PCy_3)]$ (2) (Cy = C₆H₁₁, Xyl = C₈H₉) react with 1 equiv of $[Au(PCy_3)][PF_6]$ to give $[\{Au(PCy_3)\}\{Pt_3(\mu-CNXyl)_2(\mu-CO)(CNXyl)(PCy_3)_2\}][PF_6]$ (3) and $[\{Au(PCy_3)\}\{Pt_3(\mu-CNXyl)_3(CNXyl)_2(PCy_3)\}][PF_6]$ (4), respectively. IR and multinuclear NMR data are given for 3 and 4 and related compounds. The X-ray crystal structure is given for compound 3, which crystallizes in the monoclinic space group $P2_1/m$ with $Z = 2$, $a = 14.988(13)$ Å, $b = 18.917(10)$ Å, $c = 19.28(2)$ Å, and $\beta = 67.57(6)^\circ$. The structure was refined to $R = 0.0682$ for the 3068 observed reflections ($I \geq 3\sigma(I)$).

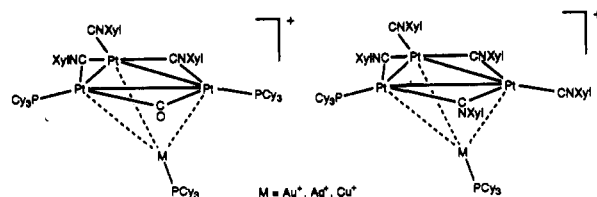
Introduction

The Lewis basicity of $[Pt_3(\mu-CO)_3(PR_3)_3]$ and $[Pt_3(\mu-CO)_3(PR_3)_4]$ toward Lewis acids like $[M(PR_3)]^+$ and $[M]^+$ ($M = Cu, Au, Ag$) can be demonstrated in the formation of heteronuclear clusters.¹⁻⁸ In all these cases the $[Pt_3(\mu-CO)_3(PR_3)_3]$ moiety reacts as a building block without undergoing major structural rearrangement itself. The addition compounds with the Lewis acid fragments lead to the formation of half-sandwich or sandwich clusters as described in the literature.¹⁻⁸ Similar Pt₃-triangular units which function also as building blocks toward $[Au(PR_3)]^+$ are $[Pt_3(\mu-SO_2)_{3-x}(\mu-L)_x(PCy_3)_3]$, $L = CNXyl$,⁹ Cl,¹⁰ SO₂,¹¹ CO,¹¹ and $[Pt_3(\mu-dppm)]_3$.¹²

Previous experiments showed that Pt and Pd clusters can be used as precursors in heterogeneous catalysis.¹³⁻¹⁵ However it is not surprising that in these systems the phosphorus of the cluster units leads to partial poisoning of the catalyst.¹⁶ In order to

study the influence of the amount of phosphorus remaining on the support toward its catalytic activity and selectivity, we investigate the synthesis of heterometallic clusters consisting of Pt₃ building blocks with different Pt:P ratios (1:1, 3:2, 3:1 and 3:0).

We now find that the formation of coordination compounds is possible with the triangular clusters $[Pt_3(\mu-CNXyl)_2(\mu-CO)(CNXyl)(PCy_3)_2]$ (1) and $[Pt_3(\mu-CNXyl)_3(CNXyl)_2(PCy_3)]$ (2).¹⁷ We have recently isolated and characterized half-sandwich and sandwich compounds with the fragments $[M(PCy_3)]^+$ with $M = Au, Ag, or Cu$.¹⁸ We report here the detailed preparation and X-ray crystal structure of the air stable, green compound $[\{Au(PCy_3)\}\{Pt_3(\mu-CNXyl)_2(\mu-CO)(CNXyl)(PCy_3)_2\}][PF_6]$ (3). NMR and IR data of the compounds 1-6 are also given.



Results and Discussion

$[\{Au(PCy_3)\}\{Pt_3(\mu-CNXyl)_2(\mu-CO)(CNXyl)(PCy_3)_2\}][PF_6]$ (3). From the reaction of the building block $[Pt_3(\mu-CNR)_2(\mu-CO)(CNR)(PCy_3)_2]$ ($R = Xyl$ (1), Cy (5)), and $[Pt_3(\mu-CNXyl)_3(CNXyl)_2(PCy_3)]$ (2) with 1 equiv of $[Au(PCy_3)][PF_6]$ the new clusters 3, 6 and 4, respectively, can be isolated. The reactions are summarized in Scheme I.

Air stable deep green crystals of 3 could be obtained by crystallization of the crude product from CH₂Cl₂/thf/petroleum ether (30-50 °C) at room temperature. The X-ray crystal structure of the compound reveals that it consists of discrete $[\{Au(PCy_3)\}\{Pt_3(\mu-CNXyl)_2(\mu-CO)(CNXyl)(PCy_3)_2\}]^+$ cations and $[PF_6]^-$ anions. ORTEP views of the metal core, as well as the carbonyl, phosphine, and isocyanide donors are shown in Figures

- * Abstract published in *Advance ACS Abstracts*, October 1, 1993.
- Briant, C. E.; Wardle, R. W. M.; Mingos, D. M. P. *J. Organomet. Chem.* **1984**, *267*, C49.
 - Albinati, A.; Dahmen, K.-H.; Togni, A.; Venanzi, L. M. *Angew. Chem.* **1985**, *97*, 760.
 - Albinati, A.; Dahmen, K.-H.; Togni, A.; Venanzi, L. M. *Angew. Chem. Int. Ed. Engl.* **1985**, *24*, 766.
 - Hallam, M. F.; Mingos, D. M. P.; Adatia, T.; McPartin, M. *J. Chem. Soc., Dalton Trans.* **1988**, 355.
 - Dahmen, K.-H. Ph.D. Thesis, ETH Zürich. **1986**, 8177.
 - Braunstein, P.; Freyburger, S.; Bars, O. *J. Organomet. Chem.* **1988**, *352*, C29.
 - Bour, J. J.; Kanters, R. P. F.; Schlebos, P. P. J.; Bos, W.; Bosman, W. P.; Behm, H.; Beurskens, P. T.; Steggerda J. J. *J. Organomet. Chem.* **1987**, *329*, 405.
 - Bhaduri, S.; Sharma, K.; Jones, P. G.; Freire Erdbrugger, C. *J. Organomet. Chem.* **1987**, *329*, C46.
 - Hill, C. M.; Mingos, D. M. P.; Powell, H.; Watson, M. J. *J. Organomet. Chem.* **1992**, *441*, 499.
 - Mingos, D. M. P.; Oster, P.; Sherman, D. J. *J. Organomet. Chem.* **1987**, *320*, 257.
 - Mingos, D. M. P.; Wardle, R. W. M. *J. Chem. Soc., Dalton Trans.* **1986**, 73.
 - Payne, N. C.; Ramachandran, R.; Schoettel, G.; Vittal, J. J.; Puddephatt, R. *J. Inorg. Chem.* **1991**, *30*, 4048.
 - Braunstein, P.; Bender, R.; Kervennal, J. *Organometallics* **1982**, 1236.
 - Baiker, A.; Dahmen, K. H.; Imhof, D.; Müller, S.; Köppel, R. (Manuscript in preparation).
 - Ichikawa, M. *J. Chem. Soc., Chem. Commun.* **1976**, 11.
 - Maire, G.; Zahraa, O.; Garin, F.; Crouzet, C.; Aeiyaach, S.; Legare, P.; Braunstein, P. *J. Chim. Phys.* **1981**, *78*, 951.

- Briant, C. E.; Gilmour, D. I.; Mingos, D. M. P.; Wardle, R. W. M. *J. Chem. Soc., Dalton Trans.* **1985**, 1693.
- Imhof, D. Ph.D. Thesis, ETH Zürich (unpublished results).

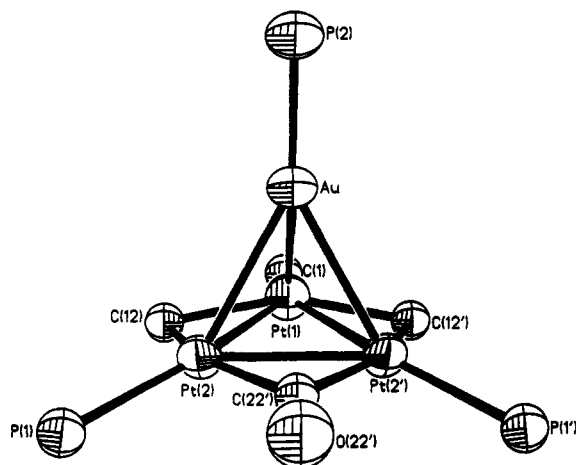


Figure 1. ORTEP view of the four metal atoms of compound $\{[\text{Au}(\text{PCy}_3)\{\text{Pt}_3(\mu\text{-CNXyl})_2(\mu\text{-CO})(\text{CNXyl})(\text{PCy}_3)_2\}][\text{PF}_6]\}$ (3).

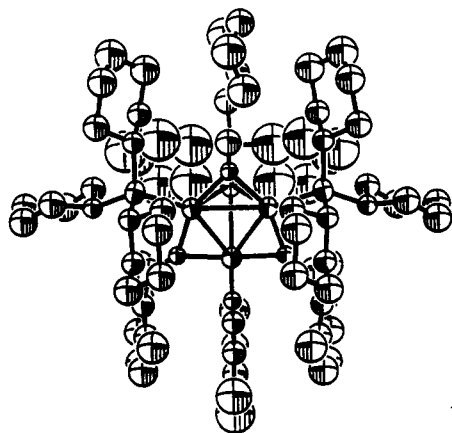
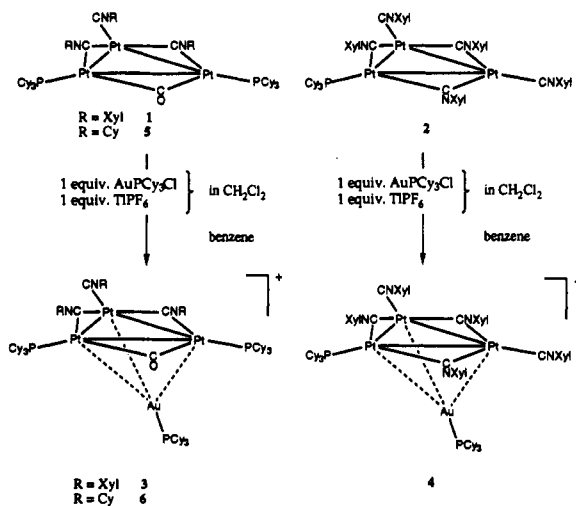


Figure 2. ORTEP view, which shows the $\{[\text{Au}(\text{PCy}_3)\{\text{Pt}_3(\mu\text{-CNXyl})_2(\mu\text{-CO})(\text{CNXyl})(\text{PCy}_3)_2\}]\}^+$ cation (3) in a nearly perfect mirror plane of symmetry.

Scheme I



1 and 2. Selected bond lengths and angles are given in Table I. The cation shows the gold atom capping the triangular array of the three platinum atoms. The cluster cation lies on a crystallographically imposed mirror plane of symmetry. All three Au-Pt distances are equal (average 2.778(2) Å). However, the Au-Pt distances are longer for 3 than for other platinum gold clusters, which are approximately equal to 2.70 Å.¹⁻⁸

Two of the Pt-Pt distances are slightly shorter (2.663(3) Å) than the third (2.681(3) Å). This result is in agreement with the

Table I. Selected Interatomic Distances (Å) and Angles (deg) of Skeletal Atoms in the Molecular Structure of $\{[\text{Au}(\text{PCy}_3)\{\text{Pt}_3(\mu\text{-CNXyl})_2(\mu\text{-CO})(\text{CNXyl})(\text{PCy}_3)_2\}][\text{PF}_6]\}$ (3) in the Crystalline State

Pt(1)-Au	2.781(4)	Pt(1)-Pt(2)	2.663(3)
Pt(2)-Au	2.777(3)	Pt(1)-Pt(2')	2.663(3)
Pt(2')-Au	2.777(3)	Pt(2)-Pt(2')	2.681(3)
Pt(2)-P(1)	2.302(8)	Pt(1)-C(1)	1.85(5)
C(1)-N(1)	1.16(7)	Pt(2)-C(12)	2.05(3)
C(12)-N(12)	1.21(4)	Pt(2)-C(22')	2.05(3)
Au-P(2)	2.257(13)	C(22')-O(22')	1.20(6)
Pt(1)-Pt(2)-Pt(2')	59.8(1)	Pt(1)-Au-Pt(2)	57.3(1)
Pt(2)-Pt(1)-Pt(2')	60.4(1)	Pt(2)-Au-Pt(2')	57.7(1)

basic unit structure of $[\text{Pt}_3(\mu\text{-CNXyl})_2(\mu\text{-CO})(\text{CNXyl})(\text{PCy}_3)_2]$ (1), in which the long Pt-Pt distance (2.648(1) Å) is bridged by a carbonyl ligand. All Pt-Pt distances for the gold phosphine capped cluster 3 are longer than for 1. However, a lengthening of the Pt-Pt was also observed in the $[\text{Pt}_3(\mu\text{-CO})_3(\text{PCy}_3)_3]$ cluster (Pt-Pt 2.655(2) Å) being capped by $[\text{AuPCy}_3]^+$ (Pt-Pt 2.696(18) Å).¹

The IR spectrum of compound 1 can be assigned according to the literature¹⁷ to terminal (2113 cm^{-1}) and bridging isocyanide (1765 cm^{-1} , 1726 cm^{-1}) ligands and also a bridging carbonyl (1803 cm^{-1}). For 3, we can clearly identify the presence of a terminal isocyanide ligand (2134 cm^{-1}). However, it is not possible to distinguish between the bridging isocyanide and the carbonyl ligands, as only two frequencies of 1725 and 1774 cm^{-1} were found in this region of the IR spectrum. Compared to 1 the carbonyl frequency is shifted to lower frequency. Therefore we can assume that in 3 the carbonyl has a higher π -back-bonding tendency.

The terminal C-N frequency shows a small shift toward higher frequencies and is therefore indicative of a higher bonding order between C and N and hence a shorter C-N bond distances in 3. This could not be confirmed from the X-ray crystal structure as the C-N bond distances, 1.18(2) Å for 1 to 1.18(7) Å for 3, are equal. For the bridging isocyanide ligand, a possible shortening of the C-N distance from 1.27(2) Å to 1.212(4) Å can be noted, but this decrease is not significant. Thus, it is concluded that there is an overlap of the CO and CN frequencies at 1774 cm^{-1} .

The $^{31}\text{P}\{^1\text{H}\}$ -NMR spectrum of 3 consists of two main patterns centered at 76.3 and 54.2 ppm. They are caused by the resonances of the phosphorus at the μ_3 -bridging $[\text{Au}(\text{PCy}_3)]^+$ moiety and by the phosphorus of the Pt_3 triangular fragment, respectively. It shows for the phosphorus on the gold atom a triplet accompanied by Pt-satellites, whereas the phosphorus on the cluster unit exhibits a doublet with Pt satellites. Due to the fact that the NMR-active ^{195}Pt has a natural abundance of 33.7%, the resulting $^{31}\text{P}\{^1\text{H}\}$ -NMR spectrum is a superposition of patterns of the various isotopomers. The spectrum of 3 has been satisfactorily simulated (Figure 3) using a computer analysis based on the following isotopomers: I, A_2M (no ^{195}Pt , 29.14%); II, $\text{AA}'\text{MX}$ (one ^{195}Pt , 29.62%); III, A_2MY (one ^{195}Pt , 14.81%); IV, $\text{AA}'\text{MXX}'$ (two ^{195}Pt , 7.53%); V, $\text{AA}'\text{MXY}$ (two ^{195}Pt , 15.06%); VI, $\text{AA}'\text{MXX}'\text{Y}$ (three ^{195}Pt , 3.82%).

The various $^2J(\text{Pt},\text{P})$ coupling constants could be analyzed from the spectrum of the isotopomers II and III, respectively. While the A part for isotopomer II ($\text{AA}'\text{MX}$ spin system) leads to an eight-line system (AKMX approximation because $^1J(\text{Pt},\text{P}) \gg ^2J(\text{Pt},\text{P})$), isotopomer III (A_2MY spin system) gives only rise to a four-line system. The coupling constants $^2J(\text{Pt}_x, \text{P}_A)$, $^2J(\text{Pt}_x, \text{P}_A')$, $^3J(\text{P}_A, \text{P}_A')$, and $^3J(\text{P}_A, \text{P}_M)$ can be determined from the first pattern and $^2J(\text{Pt}_y, \text{P}_A)$ from the latter. The chemical shifts and coupling constants for compound 3 are summarized in Table II.

As expected the $^2J(\text{Pt}_y, \text{P}_A)$ (275 Hz) and $^2J(\text{Pt}_x, \text{P}_A)$ (303 Hz) are different, while the two coupling constants $^2J(\text{Pt}_y, \text{P}_M)$ and $^2J(\text{Pt}_x, \text{P}_M)$ are equal (179 Hz). The difference in the magnitude of the former parameters is significant, whereas those

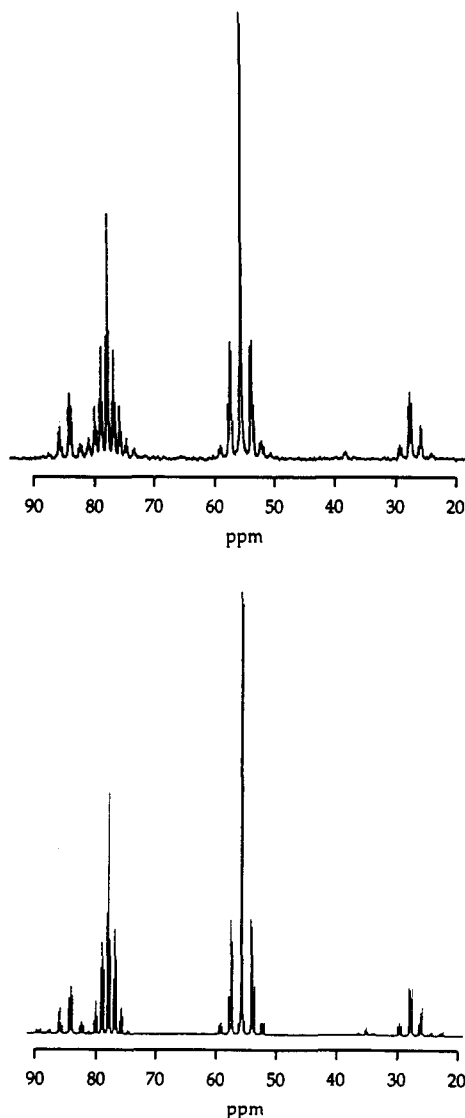


Figure 3. Phosphine section of the observed (upper) and calculated $^{31}\text{P}\{-^1\text{H}\}$ -NMR spectrum of $[\{\text{Au}(\text{PCy}_3)\}\{\text{Pt}_3(\mu\text{-CNXyl})_2(\mu\text{-CO})(\text{CNXyl})(\text{PCy}_3)_2\}][\text{PF}_6]$ (3).

found by us for the cluster unit $[\text{Pt}_3(\mu\text{-CNXyl})_2(\mu\text{-CO})(\text{CNXyl})(\text{PCy}_3)_2]$ (1) ($^2J(\text{Pt}_X, \text{P}_A) = 439$ Hz and $^2J(\text{Pt}_Y, \text{P}_A) = 435$ Hz) have to be considered equal given the experimental error and are in agreement with the literature¹⁷ (441 and 442 Hz, respectively). In the hope of finding more significant differences in these parameters, we have synthesized $[\text{Pt}_3(\mu\text{-CNCy})_2(\mu\text{-CO})(\text{CNCy})(\text{PCy}_3)_2]$ (5) and $[\{\text{Au}(\text{PCy}_3)\}\{\text{Pt}_3(\mu\text{-CNCy})_2(\mu\text{-CO})(\text{CNCy})(\text{PCy}_3)_2\}][\text{PF}_6]$ (6), which are shown in Scheme I.

Indeed, in 5 and 6 these coupling constants are clearly different and the trend is also $^2J(\text{Pt}_X, \text{P}_A) < ^2J(\text{Pt}_Y, \text{P}_A)$. This is, therefore, in good agreement with the previous interpretation of the spectra of 1 and 3. All values are given in Tables II and III, respectively.

The ^{195}Pt -NMR parameters were obtained for both 1 and 3 from conventional 1D and 2D $^{195}\text{Pt}\{-^1\text{H}\}$ correlation spectra (Figure 4) and are compiled in Tables II and III, respectively. Simulations of the 1D spectra were also successfully carried out for both compounds. The values thus obtained for 1 are in agreement with the literature¹⁷ with the exception that we compute 1050 instead of 885 Hz for $^1J(\text{Pt}_X, \text{Pt}_X)$.

Comparing the platinum shift values for 1 and 3, one notes high field displacements ($\Delta\delta$'s) of 200 and 205 ppm for the Pt_Y and Pt_X spins upon capping the platinum triangular fragment by the gold phosphine moiety. The coupling constants involving the Pt spins show an interesting trend in that the absolute values of the ones considered to be one-bond couplings, i.e. $^1J(\text{Pt}_X, \text{P})$,

Table II. $^{195}\text{Pt}\{-^1\text{H}\}$ - and $^{31}\text{P}\{-^1\text{H}\}$ -NMR Data for 3 and 6

δ (ppm)	Pt^X (Hz)	$\text{Pt}^{X'}$	Pt^Y	P^A	$\text{P}^{A'}$	P^M
R = Xyl, 3						
P^A	54.2	4665	303	275		20.2
$\text{P}^{A'}$	54.2	303	4665	275	27.8	20.2
P^M	76.3	179	179	179	20.2	20.2
Pt^X	-4530		-1855	-1040	4665	303
$\text{Pt}^{X'}$	-4530	-1855		-1040	303	4665
Pt^Y	-4070	-1040	-1040		275	275
R = Cy, 6						
P^A	51.2	4756	291	302		28.6
$\text{P}^{A'}$	51.2	291	4756	302	28.6	19.2
P^M	76.3	205	205	205	19.2	19.2

Table III. $^{195}\text{Pt}\{-^1\text{H}\}$ - and $^{31}\text{P}\{-^1\text{H}\}$ -NMR Data for 1 and 5

δ (ppm)	Pt^X (Hz)	$\text{Pt}^{X'}$	Pt^Y	P^A	$\text{P}^{A'}$
R = Xyl, 1					
P^A	71.3	4098	435	439	
$\text{P}^{A'}$	71.3	435	4098	439	57.0
Pt^X	-4325		-1050	-325	4098
$\text{Pt}^{X'}$	-4325	-1050		-325	435
Pt^Y	-3870	-325	-325		439
R = Cy, 5					
P^A	72.0	4217	441	460	
$\text{P}^{A'}$	72.0	441	4217	460	57.0

$^1J(\text{Pt}_X, \text{Pt}_X)$, and $^1J(\text{Pt}_X, \text{Pt}_Y)$, increase significantly, whereas those of two-bond couplings, i.e. $^2J(\text{Pt}_X, \text{P})$ and $^2J(\text{Pt}_Y, \text{P})$, decrease.

The large increase in the Pt–Pt coupling constants from -1050 to -1855 Hz and from -325 to -1040 Hz for $^1J(\text{Pt}_X, \text{Pt}_X)$ and $^1J(\text{Pt}_X, \text{Pt}_Y)$, respectively, seems to contradict the idea of weaker metal–metal bonds in the tetrahedral type cluster 3 as opposed to 1. The expectation of weaker bonds in 3 is implied by X-ray analysis showing longer Pt–Pt separations in 3. However, there is no straightforward relationship between the magnitudes of coupling constants and bond lengths; attempts to correlate $^1J(\text{Pt}, \text{Pt})$ values with bond lengths in clusters failed. In addition, it had been shown^{18,19} by ^{195}Pt – ^{31}P heteronuclear multiple-quantum spectroscopy (HMQC) that the coupling constants $^1J(\text{Pt}, \text{Pt})$ in $[\text{Pt}_3(\mu\text{-CO})_3(\text{PR}_3)_3]$ are negative. These negative signs had been interpreted in terms of significant contributions from the geminal coupling pathway via the bridging carbonyl ligands.

The feasibility of metal–proton heteronuclear multiple quantum

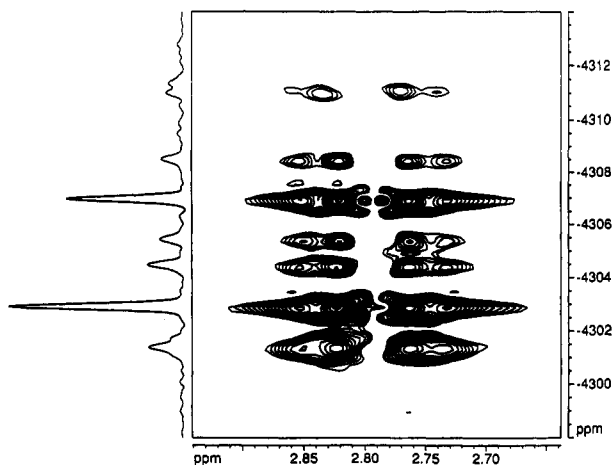


Figure 4. Section of the $^{195}\text{Pt}-^1\text{H}$ HMQC spectrum (11.7 T, $\Delta = 8$ ms) recorded for **1**, showing details in the cross peak between the H-C(α) resonance of PCy_3 and the low field wing of the Pt_X resonance. The conventional $^{195}\text{Pt}\{^1\text{H}\}$ -NMR spectrum is plotted at the left.

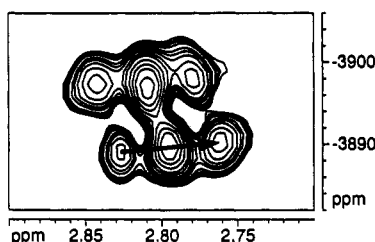


Figure 5. Section of the $^{195}\text{Pt}-^1\text{H}$ HMQC spectrum (11.7 T, $\Delta = 80$ ms) recorded for **1**, showing the cross peak due to the Pt_Y resonance. The vertical splitting in the 2D multiplet corresponds to $2^2J(\text{Pt}_Y, \text{P}_A)$. The arrow, which links the Pt satellites due to the Pt_X spin, has the components $^3J(\text{Pt}_X, \text{H}-\text{C}(\alpha))$ in F_2 (^1H , horizontal) and $\Sigma J(\text{Pt}_X, \text{Pt}_Y) + ^2J(\text{Pt}_Y, \text{P}_A) = -325 + 439 = 114$ Hz, in F_1 (^{195}Pt), respectively.

spectroscopy for unraveling metal NMR parameters^{20,21} has been assessed for $[\text{Pt}_3(\mu\text{-CNXyl})_2(\mu\text{-CO})(\text{CNXyl})(\text{PCy}_3)_2]$ (**1**), in the hope of gaining additional insights into this class of compounds. This type of experiment, performed for $^{195}\text{Pt}-^1\text{H}$ and tuned to the coupling ($^3J(\text{Pt}, \text{H})$) between the α -proton of the cyclohexyl and Pt_X , reproduced extremely well the features of the conventional platinum spectrum, as can be judged from Figure 4. Unfortunately, little additional information, e.g. with respect to signs of coupling constants, can be discerned. This arises in particular because of the small magnitudes of couplings to remote platinum spins. However, if the same experiment is performed in a way that such long range interactions are emphasized, supplementary information may be obtained (Figure 5 showing the cross peak between the H-C(α) and the Pt_Y resonances). While the conventional 1D $^{195}\text{Pt}\{^1\text{H}\}$ spectrum shows a broad, more or less featureless multiplet, the HMQC exhibits a nicely resolved and simple pattern. This behavior seems to be unexpected at first, however, since the dominant spin systems responsible for the conventional $^{195}\text{Pt}\{^1\text{H}\}$ spectrum have a first order appearance (triplet and doublet of doublet for the A_2Y and $\text{AA}'\text{XY}$ spin systems, respectively), while the HMQC experiment excites those of second-order types because the protons are not decoupled. Thus the A_2Y type transforms into $\text{AA}'\text{H}_3\text{H}'_3\text{Y}$. Its main consequence^{17,22,23} with respect to the spectrum depicted in Figure 5 consists of the following: (i) the original triplet due to the interaction with two ^{31}P spins in the platinum spectrum reduces

to its outer two lines and this is essentially the origin of the "higher" resolution; (ii) the platinum satellites due to the Pt_X spins are well separated in the ^1H dimension, because the latter has a large coupling (ca. +33 Hz) to the vicinal H-C(α) protons. In the platinum dimension their separation is small (ca. 120 Hz) and corresponds to the sum of $^1J(\text{Pt}_X, \text{Pt}_Y)$ and $^2J(\text{Pt}_Y, \text{P})$.

The magnitudes of these two parameters (325 and 439 Hz) are known from the X part of the ^{195}Pt and the ^{31}P spectra, respectively. On the basis that the vicinal coupling constant $^3J(\text{Pt}_X, \text{H}-\text{C}(\alpha))$ has a positive sign, it has to be deduced that $^2J(\text{Pt}_Y, \text{P})$ is positive while $^1J(\text{Pt}_X, \text{Pt}_Y)$ is negative. This conclusion is in agreement with results previously obtained for the clusters $[\text{Pt}_3(\mu\text{-CO})_3(\text{PR}_3)_3]$.¹⁹

A similar experiment performed for the gold-containing cluster **3** failed, presumably due to a combination of faster relaxation of the $^{195}\text{Pt}_Y$ spin and/or smaller coupling constants $^4J(\text{Pt}_Y, \text{H}-\text{C}(\alpha))$. The former assumption might be supported by a general increase in the line width in the ^{195}Pt resonances whereas the latter might be related to the decrease of the corresponding $^2J(\text{Pt}_Y, \text{P}_A)$ when going from **1** to **3**. Acceptable results should be obtainable by using $^{195}\text{Pt}-^{31}\text{P}$ HMQC techniques. Corresponding experiments are in progress.

$\{[\text{Au}(\text{PCy}_3)]\{[\text{Pt}_3(\mu\text{-CNXyl})_3(\text{CNXyl})_2(\text{PCy}_3)]\}[\text{PF}_6]\}$ (**4**). A second type of a half-sandwich cluster has been synthesized by the reaction of $[\text{Au}(\text{PCy}_3)]^+$ with **2**. Comparing the structure of $\{[\text{Au}(\text{PCy}_3)]\{[\text{Pt}_3(\mu\text{-CNXyl})_2(\mu\text{-CO})(\text{CNXyl})(\text{PCy}_3)_2]\}[\text{PF}_6]\}$ (**3**) and $\{[\text{Au}(\text{PCy}_3)]\{[\text{Pt}_3(\mu\text{-CNXyl})_3(\text{CNXyl})_2(\text{PCy}_3)]\}[\text{PF}_6]\}$ (**4**), one notes that in the latter the carbonyl and one of the phosphine ligands have been replaced by a bridging and a terminal isocyanide ligand, respectively. As a consequence of the lower number of phosphorus spins, the NMR spectra of **4** are much simpler. In the $^{31}\text{P}\{^1\text{H}\}$ -NMR spectrum the main resonances for the phosphorus on the gold and the phosphorus on the platinum fragment are both doublets with appropriate Pt satellites resulting from one and two bond Pt-P couplings.

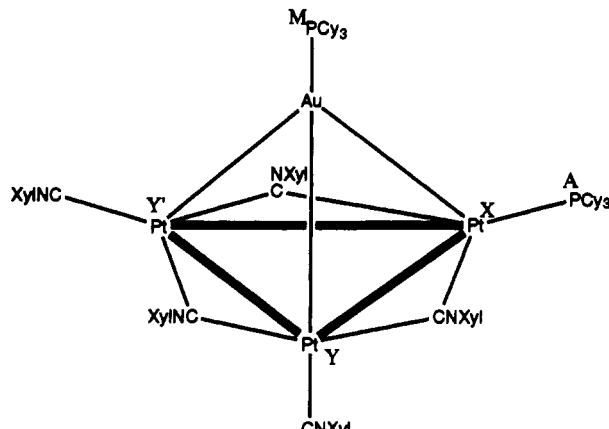
The complete pattern, being again the superposition of the subspectra of the isotopomers, has been satisfactorily simulated using a computer analysis based on the following isotopomers: I, AM (no ^{195}Pt , 29.14%); II, AMX (one ^{195}Pt , 14.81%); III, AMY (one ^{195}Pt , 29.63%); IV, AMXY (two ^{195}Pt , 15.06%); V, AMY₂ (two ^{195}Pt , 7.53%); VI, AMY₂X (three ^{195}Pt , 3.82%). The $^{195}\text{Pt}\{^1\text{H}\}$ -NMR spectrum is of first order for all of the relevant isotopomers and consists of doublets of doublets for both the Pt_Y and Pt_X resonances flanked by the appropriate Pt satellites of the other Pt spins. The relevant coupling constants and chemical shifts can easily be determined from there and are given in Table IV.

It is worth noting that for **4** the two coupling constants $^2J(\text{Pt}_Y, \text{P}_M)$ (237 Hz) and $^2J(\text{Pt}_X, \text{P}_M)$ (270 Hz) are clearly different, while those for **3** and **6** are equal. The IR spectrum of $[\text{Pt}_3(\mu\text{-CNXyl})_3(\text{CNXyl})_2(\text{PCy}_3)]$ (**2**) shows both terminal (2313 and 2100 cm^{-1}) and bridging (1704 cm^{-1}) isocyanide ligands. The coordination of a gold phosphine cation leads to a shift of terminal isocyanide C-N stretching frequencies to lower frequencies (2126 and 1972 cm^{-1}) and to a slightly higher frequency (1713 cm^{-1}) for the bridging isocyanide ligands. These tendencies of shifts are different from the previous discussion of **1** and **3**.

Furthermore we have tried to prepare the analogous cluster of **3** and **4** using $[\text{Pt}_3(\mu\text{-CNXyl})_3(\text{CNXyl})_3]$ ²⁴ as building block. We have noticed from the NMR that it might be possible to synthesize a heterometallic cluster.¹⁸ Experiments to isolate this species are under investigation. However it can be noted that the stability of the different heterometallic gold Pt_3 clusters decreases in the order of $[\text{Pt}_3(\mu\text{-CO})_3(\text{PCy}_3)_3] > [\text{Pt}_3(\mu\text{-CNXyl})_2(\mu\text{-CO})(\text{CNXyl})(\text{PCy}_3)_2]$ (**1**) $>$ $[\text{Pt}_3(\mu\text{-CNXyl})_3(\text{CNXyl})_2(\text{PCy}_3)]$ (**2**) $>$ $[\text{Pt}_3(\mu\text{-CNXyl})_3(\text{CNXyl})_3]$.

(20) Imhof, D.; Rügger, H.; Venanzi, L. M.; Ward, T. R. *Magn. Reson. Chem.* **1991**, *29*, S73.
 (21) Templeton, J. L.; Philipp, C. C.; Pregosin, P. S.; Rügger, H. *Magn. Reson. Chem.* **1993**, *31*, 58.
 (22) Nanz, D.; Von Philipsborn, W. J. *Magn. Reson.* **1991**, *92*, 560.
 (23) Braunschweiler, L.; Bodenhauser, G.; Ernst, R. R. *Mol. Phys.* **1983**, *3*, 535.

(24) Green, M.; Howard, J. A. K.; Murray, M.; Spencer, J. L.; Stone, F. G. A. *J. Chem. Soc., Dalton Trans.* **1977**, 1509.

Table IV. $^{195}\text{Pt}\{^1\text{H}\}$ - and $^{31}\text{P}\{^1\text{H}\}$ -NMR Data for 4


	δ (ppm)	Pt ^X (Hz)	Pt ^{X'}	Pt ^Y	P ^A	P ^M
P ^A	45.9	323	323	4401		20
P ^M	73.2	270	270	237	20	
Pt ^X	-4075			-924	323	270
Pt ^{X'}	-4075			-924	323	270
Pt ^Y	-4785	-924	-924		4401	237

Table V. Experimental Data for the X-ray Diffraction Studies of $\{[\text{Au}(\text{PCy}_3)]\{[\text{Pt}_3(\mu\text{-CNXyl})_3(\mu\text{-CO})(\text{CNXyl})(\text{PCy}_3)_2]\}\}[\text{PF}_6] (3)$

formula	$\text{C}_{82}\text{H}_{128}\text{ON}_3\text{P}_4\text{AuPt}_3\text{F}_6$	Z	2
mol wt	2192	ρ_{calc} , g cm ⁻³	1.441
cryst syst	monoclinic	μ , cm ⁻¹	56.98
space group	$P2_1/m$	T, °C	25
a, Å	14.988(13)	λ , Å	0.71073 (graphite monochromated, Mo K α)
b, Å	18.917(10)	R^a	0.0682
c, Å	19.28(2)	R_w^b	0.0745
β , deg	67.57(6)	GOF	1.22
V, Å ³	5053(7)		

^a $R = \sum(|F_o| - 1/k|F_d|) / \sum|F_o|$. ^b $R_w = [\sum(|F_o| - 1/k|F_d|)^2 / \sum w|F_o|^2]^{1/2}$, where $w = [\sigma^2(F_o)]^{-1}$.

Conclusions

The clusters $[\text{Pt}_3(\mu\text{-CNXyl})_2(\mu\text{-CO})(\text{CNXyl})(\text{PCy}_3)_2]$ (1) and $[\text{Pt}_3(\mu\text{-CNXyl})_3(\text{CNXyl})_2(\text{PCy}_3)]$ (2) are useful building blocks for the preparation of heterometallic clusters. Even the $[\text{Pt}_3(\mu\text{-CNXyl})_3(\text{CNXyl})_3]$ cluster without any phosphines might be a potential starting material for new clusters. However the stability of the addition products with Lewis acids seem to decrease by higher substitution of phosphine ligands with isocyanide ligands.

Experimental Part

Reactions were routinely carried out using standard Schlenk line procedures under an atmosphere of pure argon and using dry O₂-free solvents. The compounds $[\text{Au}(\text{PCy}_3)\text{Cl}]$ and $[\text{Pt}_3(\mu\text{-CO})_3(\text{PCy}_3)_3]$ were prepared as described in the literature.^{25,26} A modification of the synthesis of the compounds $[\text{Pt}_3(\mu\text{-CNXyl})_2(\mu\text{-CO})(\text{CNXyl})(\text{PCy}_3)_2]$ (1) and $[\text{Pt}_3(\mu\text{-CNXyl})_3(\text{CNXyl})_2(\text{PCy}_3)]$ (2) are given here. Infrared spectra were recorded on a Perkin-Elmer 883 spectrometer as RbI pellets. $^{31}\text{P}\{^1\text{H}\}$ -NMR spectra were run on a Bruker AC250 spectrometer for compounds 1, 2, 4, and 5 and on a Bruker AC200 spectrometer for compounds 3 and 6. The ^{31}P operating frequencies were 101.3 and 81.0 MHz, respectively. $^{31}\text{P}\{^1\text{H}\}$ -NMR simulations were carried out using a program developed by Rappé.²⁷

¹H and $^{195}\text{Pt}\{^1\text{H}\}$ spectra were recorded on a Bruker AMX 500 spectrometer operating at 500.1 and 107.5 MHz, respectively. ^{195}Pt , ¹H heteronuclear multiple quantum spectra were measured using the

Table VI. Atomic Coordinates ($\times 10^4$) and Equivalent Isotropic Displacement Coefficients ($\text{Å}^2 \times 10^3$)

	x	y	z	U(eq) ^a
Pt(1)	9759(1)	7500	3193(1)	51(1)
Pt(2)	8317(1)	6792(1)	3029(1)	44(1)
C(1)	10801(29)	7500	3488(22)	41(12)
N(1)	11550(29)	7500	3540(21)	70(12)
C(111)	12448(39)	7500	3688(32)	80(16)
C(112)	12303(41)	7500	4480(33)	85(17)
C(113)	13149(67)	7500	4588(58)	223(42)
C(114)	13981(48)	7500	3957(39)	115(22)
C(115)	14200(43)	7500	3261(36)	100(19)
C(116)	13274(48)	7500	3130(38)	109(20)
C(117)	11429(46)	7500	5061(38)	175(32)
C(118)	13277(42)	7500	2382(33)	140(27)
C(12)	9443(19)	6481(14)	3314(15)	38(8)
N(12)	9802(19)	5941(16)	3424(15)	83(9)
C(121)	10605(23)	5780(16)	3670(20)	66(10)
C(122)	10418(26)	5861(18)	4399(22)	82(11)
C(123)	11255(29)	5763(20)	4650(26)	117(15)
C(124)	12084(31)	5645(20)	4053(24)	111(14)
C(125)	12315(29)	5574(19)	3316(24)	106(14)
C(126)	11463(30)	5662(21)	3061(25)	104(14)
C(127)	9547(27)	6040(21)	5045(22)	127(16)
C(128)	11585(30)	5618(22)	2332(23)	140(18)
P(1)	7358(6)	5798(4)	3270(5)	52(4)
C(211)	6527(20)	5768(15)	4271(15)	52(9)
C(212)	5835(22)	6388(16)	4517(17)	68(10)
C(213)	5103(25)	6341(20)	5285(18)	94(13)
C(214)	5678(24)	6380(17)	5780(19)	81(11)
C(215)	6424(24)	5783(17)	5621(19)	87(12)
C(216)	7075(20)	5811(16)	4767(16)	57(9)
C(221)	6561(20)	5801(16)	2793(16)	54(9)
C(222)	5839(22)	5193(17)	2948(19)	78(11)
C(223)	5090(25)	5347(20)	2575(20)	94(13)
C(224)	5550(28)	5450(21)	1748(22)	119(15)
C(225)	6326(26)	6012(20)	1526(22)	104(14)
C(226)	7075(22)	5870(17)	1917(17)	69(10)
C(231)	8065(19)	4971(14)	3146(16)	47(8)
C(232)	8811(23)	4909(17)	2331(18)	79(11)
C(233)	9479(26)	4317(18)	2301(22)	105(14)
C(234)	8958(25)	3614(18)	2592(19)	91(12)
C(235)	8190(25)	3691(19)	3338(20)	98(13)
C(236)	7486(24)	4293(16)	3413(20)	86(12)
C(22')	7385(29)	7500	2865(22)	37(11)
O(22')	6642(23)	7500	2765(18)	79(11)
Au	9618(1)	7500	1796(1)	58(1)
P(2)	10333(9)	7500	532(8)	67(6)
C(411)	9481(29)	7437(46)	119(23)	92(22)
C(412)	8474(33)	7773(42)	565(17)	142(37)
C(413)	7730(22)	7507(44)	238(25)	158(28)
C(414)	8074(28)	7720(42)	-606(25)	107(29)
C(415)	9081(35)	7383(44)	-1052(20)	160(36)
C(416)	9825(21)	7649(50)	-725(21)	80(22)
C(421)	11031(31)	6678(17)	81(25)	262(15)
C(422)	11849(32)	6646(23)	394(29)	262(15)
C(423)	12471(26)	5968(24)	95(33)	262(15)
C(424)	11944(30)	5462(19)	-262(22)	262(15)
C(425)	10882(30)	5346(18)	296(30)	262(15)
C(426)	10312(21)	6055(24)	411(32)	262(15)
P(3)	6436(14)	2500	2188(13)	146(15)
F(1)	6605(28)	3345(22)	2196(22)	256(20)
F(2)	6512(35)	2500	3002(31)	213(20)
F(3)	7567(34)	2500	1815(25)	193(18)
F(4)	5402(46)	2500	2461(33)	255(25)
F(5)	6469(28)	2500	1361(25)	161(15)

^a Equivalent isotropic U defined as one-third of the trace of the orthogonalized U_{ij} tensor.

sequence²⁸ $\pi/2$ (¹H)- Δ - $\pi/2$ (^{195}Pt)- $t_{1/2}$ - π (¹H)- $t_{1/2}$ - $\pi/2$ (^{195}Pt)-Acq (¹H), where Δ was set to 8 and 80 ms for emphasizing "direct" (HCPtPt) or long range (HCPPtPt) interactions, respectively. $^{31}\text{P}\{^1\text{H}\}$ -NMR and $^{195}\text{Pt}\{^1\text{H}\}$ -NMR were measured and reported by using H₃PO₄ (85%) as an internal standard and Na₂PtCl₆, respectively.

Preparation of $[\text{Pt}_3(\mu\text{-CNXyl})_2(\mu\text{-CO})(\text{CNXyl})(\text{PCy}_3)_2]$ (1). $[\text{Pt}_3(\mu\text{-CO})_3(\text{PCy}_3)_3]$ (0.500 g, 0.331 mmol) was dissolved in thf (50 cm³).

(25) McAuliffe, C. A.; Parish, R. V.; Randall, P. D. *J. Chem. Soc., Dalton Trans.* 1979, 1730.

(26) Clark, H. C.; Goel, A. B.; Wang, C. S. *Inorg. Chim. Acta* 1979, 34, 159.

(27) Rappé, A. K. Colorado State University; Casewit, L. J. Calleo Scientific Software Publishers, 1989.

(28) Summers, M. F.; Marzilli, L. G.; Bax, A. *J. Am. Chem. Soc.* 1986, 108, 4285.

A solution of CNXyl (0.152 g, 1.152 mmol) in CH_2Cl_2 (3 cm^3) was slowly added and vigorous stirring continued for 30 min, after which time an orange microcrystalline solid had formed. The solid was isolated and washed with cold methanol to give orange crystals of **1** in 65% yield. Anal. Calcd for $\text{C}_{64}\text{H}_{93}\text{N}_3\text{OP}_2\text{Pt}_3$: C, 49.04; H, 5.98; N, 2.68. Found: C, 48.65; H, 5.96; N, 2.31. IR: $\nu(\text{CN})$ at 2113, 1765, 1726, and 1681 cm^{-1} ; $\nu(\text{CO})$ at 1803 cm^{-1} .

Preparation of $[\text{Pt}_3(\mu\text{-CNCy})_2(\mu\text{-CO})(\text{CNCy})(\text{PCy}_3)_2]$ (5**).** $[\text{Pt}_3(\mu\text{-CO})_3(\text{PCy}_3)_3]$ (0.500 g, 0.331 mmol) was dissolved in thf (50 cm^3). A solution of CNCy (145 μL , 1.191 mmol) in thf (10 cm^3) was slowly added and vigorous stirring continued for 40 min. The resulting solution was concentrated in vacuo and pentane added to precipitate the product as orange microcrystals of **5** in 50% yield. Anal. Calcd for $\text{C}_{58}\text{H}_{99}\text{N}_3\text{OP}_2\text{Pt}_3$: C, 46.39; H, 6.65; N, 2.80. Found: C, 47.09; H, 6.83; N, 2.40. IR: $\nu(\text{CN})$ at 2115, 1727, 1694, and 1614 cm^{-1} ; $\nu(\text{CO})$ at 1799 cm^{-1} .

Preparation of $[\{\text{Au}(\text{PCy}_3)\}\{\text{Pt}_3(\mu\text{-CNXyl})_2(\mu\text{-CO})(\text{CNXyl})(\text{PCy}_3)_2\}]\text{PF}_6$ (3**).** $[\text{Pt}_3(\mu\text{-CNXyl})_2(\mu\text{-CO})(\text{CNXyl})(\text{PCy}_3)_2]$ (**1**) (0.050 g, 0.032 mmol) was dissolved in benzene (5 cm^3). A solution of TIPF_6 (0.011 g, 0.032 mmol) and $[\text{Au}(\text{PCy}_3)\text{Cl}]$ (0.016 g, 0.032 mmol) in CH_2Cl_2 (1 cm^3) was added with stirring. The color changed immediately from light red to dark green and, after stirring for 40 min, a green solid had formed. Isolation and recrystallization from CH_2Cl_2 and petroleum ether gave deep green crystals of **3** in 70% yield. Anal. Calcd for $\text{C}_{82}\text{H}_{126}\text{N}_3\text{OF}_6\text{P}_4\text{Pt}_3\text{Au}$: C, 44.97; H, 5.80; N, 1.92. Found: C, 44.71; H, 5.58; N, 1.79. IR: $\nu(\text{CN})$ at 2134 cm^{-1} ; $\nu(\text{CN and/or CO})$ at 1725, 1586, and 1774 cm^{-1} . Crystals suitable for X-ray diffraction were prepared by slow diffusion of petroleum ether (30–50 °C) into a CH_2Cl_2 /thf solution of **3**.

Preparation of $[\{\text{Au}(\text{PCy}_3)\}\{\text{Pt}_3(\mu\text{-CNCy})_2(\mu\text{-CO})(\text{CNCy})(\text{PCy}_3)_2\}]\text{PF}_6$ (6**).** $[\text{Pt}_3(\mu\text{-CNCy})_2(\mu\text{-CO})(\text{CNCy})(\text{PCy}_3)_2]$ (**5**) (0.050 g, 0.033 mmol) was dissolved in CH_2Cl_2 (10 cm^3). A solution of TIPF_6 (0.012 g, 0.034 mmol) and $[\text{Au}(\text{PCy}_3)\text{Cl}]$ (0.017 g, 0.033 mmol) in thf (1 cm^3) was added with stirring. The color changed immediately from light red to dark green. The resulting solution was concentrated in vacuo and pentane added to precipitate the product as green microcrystals of **6** in 70% yield. Anal. Calcd for $\text{C}_{76}\text{H}_{132}\text{N}_3\text{OF}_6\text{P}_4\text{Pt}_3\text{Au}$: C, 42.98; H, 6.26; N, 1.98. Found: C, 42.32; H, 6.17; N, 1.83. IR: $\nu(\text{CN})$ at 2167 cm^{-1} ; $\nu(\text{CN and/or CO})$ 1750 and 1617 and 1773 cm^{-1} .

Preparation of $[\text{Pt}_3(\mu\text{-CNXyl})_3(\text{CNXyl})_2(\text{PCy}_3)]$ (2**).** $[\text{Pt}_3(\mu\text{-CO})_3(\text{PCy}_3)_3]$ (0.200 g, 0.132 mmol) was dissolved in thf (20 cm^3). A solution of CNXyl (0.087 g, 0.662 mmol) in thf (5 cm^3) was slowly added and vigorous stirring continued for 20 min. The resulting solution was concentrated in vacuo and methanol added to precipitate the product as red crystals of **2** in 33% yield. Anal. Calcd for $\text{C}_{63}\text{H}_{73}\text{N}_3\text{PPt}_3$: C, 49.90; H, 4.85; N, 4.62. Found: C, 49.55; H, 5.29; N, 4.16. IR: $\nu(\text{CN})$ at 2100, 1704, and 1582 cm^{-1} .

Preparation of $[\{\text{Au}(\text{PCy}_3)\}\{\text{Pt}_3(\mu\text{-CNXyl})_3(\text{CNXyl})_2(\text{PCy}_3)\}]\text{PF}_6$ (4**).** $[\text{Pt}_3(\mu\text{-CNXyl})_3(\text{CNXyl})_2(\text{PCy}_3)]$ (**2**) (0.050 g, 0.033 mmol) was dissolved in benzene (10 cm^3). A solution of TIPF_6 (0.011 g, 0.033 mmol) and $[\text{Au}(\text{PCy}_3)\text{Cl}]$ (0.017 g, 0.033 mmol) in thf (1 cm^3) was added with stirring. The color changed immediately from light red to dark green. The resulting solution was concentrated in vacuo and pentane added to precipitate the product as green microcrystals of **4** in 92% yield. Anal. Calcd for $\text{C}_{81}\text{H}_{111}\text{N}_3\text{F}_6\text{P}_4\text{Pt}_3\text{Au}$: C, 45.38; H, 5.22; N, 3.27. Found: C, 45.15; H, 4.95; N, 3.13. IR: $\nu(\text{CN})$ at 2126, 1972, 1713, and 1584 cm^{-1} .

Crystallography. A deep green crystal having the form of a thin platelet (0.2 × 0.2 × 0.08 mm) was put on a Nicolet R3M diffractometer which was then used for the determination of lattice parameters, space group, and data collection. The cell parameters were obtained by a least-squares fit of the 2θ values of 20 high-angle reflections ($19.1^\circ \leq 2\theta \leq 22.0^\circ$). The crystallographic data are listed in Table V.

A total of 5180 reflections were measured in the 2θ -range of 3–45°. During data collection one standard reflection (1,2,1) was measured every 200 reflections; no significant variations of the intensities were observed. Data were corrected by Lorentz and polarization factors and by numerical face indexed absorption correction. Reflections at high 2θ values above 40° showed a very low intensity because of the poor quality of the crystal. Reflections having $I \geq 3\sigma(I)$ were considered as observed and thus 3068 reflections were used for the solution and refinement of the structure.

The structure was solved by Patterson and difference Fourier methods using the SHELXTL-PLUS system. Refinement was carried out by full matrix least squares; the function minimized was $\sum w(|F_o| - |kF_c|)^2$. The structure was refined using the centrosymmetric space group $P2_1/m$ even though this symmetry is incompatible with the PCy_3 unit bonded to Au. The carbon atoms of these groups have huge temperature displacement parameters. One cyclohexyl group lies very close to the mirror plane, it was refined as a rigid group having the ideal geometry of cyclohexyl. An occupancy factor of 0.5 was used such that the two symmetrical positions yielded a full occupancy of 1.0. The other two groups, which are equivalent in $P2_1/m$, were also refined as rigid cyclohexyls; in addition the thermal displacement parameters of the carbon atoms in these groups were fixed together and refined as a single parameter. However, the average structure is perfectly centrosymmetric. Attempts to use the noncentrosymmetric space group $P2_1$ yielded a slightly lower R value of 0.0662 versus 0.0682. The data set is not sufficient to make a clear decision whether the crystal structure is noncentrosymmetric $P2_1$ or centrosymmetric $P2_1/m$ with some disorder. Because of simplicity it was refined in the centrosymmetric space group. The positions of the hydrogen atoms were calculated but not refined. Anisotropic temperature factors were used for Pt, Au, and P atoms; all others were refined isotropically. Scattering factors were taken from ref 29. The final positions of the atoms are listed in Table VI.

Acknowledgment. We gratefully acknowledge the support of the Schweizerischer Schulrat.

Supplementary Material Available: Listings of experimental $^{31}\text{P}\{^1\text{H}\}$ - and $^{195}\text{Pt}\{^1\text{H}\}$ -NMR spectra of compounds **1**, **2**, **4**, and **5** (Figures S1–S4) and **1**, **3**, and **4**, respectively (Figures S5–S7), calculated $^{31}\text{P}\{^1\text{H}\}$ - and $^{195}\text{Pt}\{^1\text{H}\}$ -NMR spectra of compounds **4** (Figure S8) and **1**, **3**, and **4**, respectively (Figures S9–S11), structure determination summary, data collection, solution and refinement, tables of atomic coordinates and equivalent isotropic displacement coefficients, complete bond lengths and bond angles, anisotropic displacement coefficients, H-atom coordinates and isotropic displacement coefficients (22 pages). Ordering information is given on any current masthead page. Inquires for copies of these materials as also for tables of observed and calculated structure factors (18 pages) can be directed to the corresponding authors.

(29) *International Tables for X-ray Crystallography*; Kynoch Press: Birmingham, England, 1974.